New Hybrid Fe-based MOF/polymer Composites for the photodegradation of organic dyes

Chaima Brahmi, Mahmoud Benltifa, Cyril Vaulot, Laure Michelin, Frédéric Dumur, Effrosyni Gkaniatsou, Clémence Sicard, Aissam Airoudj, Fabrice Morlet-savary, Latifa Bousselmi, et al.

▶ To cite this version:

Chaima Brahmi, Mahmoud Benltifa, Cyril Vaulot, Laure Michelin, Frédéric Dumur, et al.. New Hybrid Fe-based MOF/polymer Composites for the photodegradation of organic dyes. ChemistrySelect, 2021, 6 (31), pp.8120-8132. 10.1002/slct.202102194 . hal-03334725

HAL Id: hal-03334725
https://hal.science/hal-03334725v1

Submitted on 4 Sep 2021

New Hybrid Fe-based MOF/polymer Composites for the photodegradation of organic dyes

Chaima Brahmi[a,b,c,d], Mahmoud Benltifa*[c], Cyril Vaulot[a,b], Laure Michelin[a,b], Frédéric Dumur [e], Effrosyni Gkaniatsou [f], Clémence Sicard [f], Aissam Airoudj[a,b], Fabrice Morlet-Savary[a,b], Latifa Bousselmi[c], Jacques Lalevée* [a,b]

[a] University of Haute-Alsace, CNRS, IS2M UMR 7361, F-68100 Mulhouse, France

[b] University de Strasbourg, France

[c] Laboratory of Wastewaters and Environment, Center for Water Research and Technologies CERTE, BP 273, Soliman 8020, Tunisia

[d] University of Carthage, National Institute of Applied Sciences and Technology, Tunis 1080, Tunisia
[e] Aix Marseille Univ, CNRS, ICR, UMR7273, F-13397 Marseille (France)
[f] Institut Lavoisier Versailles, UMR CNRS 8180, Université de Versailles-St-Quentin-en-Yvelines, 45 Avenue des États-Unis, 78035 Versailles cedex, France

*Corresponding author: Jacques.lalevee@uha.fr and mahmoud.benltifa@certe.rnrt.tn

Abstract

Metals Organic Frameworks (MOFs) are promising crystalline, embrittled materials generally produced in powdering form with varied remarkably functionalities. In contrary, polymer are flexible and processable materials. Therefore, obtaining shaped solids gathering polymer malleability and MOFs properties such as their photocatalytic activities, have attracked many reasearchers attention. This work, report the successful fruitful incorporation of two different Fe-based MOFs into a polymer matrix via a facile and cheap photopolymerization process upon mild visible light irradiation at 405 nm. The as-prepared photocomposites displayed excellent stability and photocalytic performance for several Acid Black degradation cycles. Hence, approximatively, 95% of this model dye was decomposed by the two MIL-100(Fe)/polymer and MIL-88A(Fe)/polymer composites under juste 30 min of UV lamp irradiation. Incorporation of the MOFs into the polymer was confirmed by several techniques including Scanning Electron Microscopy (SEM), Energy-dispersive X- ray analysis

(EDX), Transmission Electron Microscopy (TEM), X- Ray Diffraction analysis (DRX), Fourier-Transform Infrared Spectroscopy (FTIR). Furthermore, these photocatalysts exhibited a high thermal stability, excellent rigidity and low band gap energy characterized by Thermogravimetric Analysis (TGA) Atomic Force Microscopy (AFM), Dynamic Mechanical Analysis (DMA) and UV-Visible diffuse reflectance spectroscopy, respectively.

1. Introduction

Metal Organic Frameworks are a class of porous and crystalline materials that have captivated attention of many researchers during the last few decades. These hybrid inorganic/organic solids are constituted by metal or metal clusters connected in a three dimensional structure by polyfunctional organic molecules[1,2]. Thanks to the countless possible combinations between metal ions and ligands, numerous MOFs can be designed and developed with specific properties depending on the desired applications[2]. Indeed, the different flexible chemical and physical properties of MOFs including their huge surface area, high controllable internal volume and chemical stability, have allowed their applications in several fields such as separation processes[3], biomedicine[4], gas storage[5], photoluminescence[6] and catalysis[7].

Thanks to their semiconductor's properties, MOFs have been recently used for removing different organic pollutants such as dyes[8], pesticides[9], pharmaceuticals[9,10], personal care products[9] and heavy metals[11] from water effluents. In fact, the photocatalytic behavior of these materials emerges from the coordination between the metal and the oxygen of the ligand forming metal-oxide cluster which could exhibit photocatalytic performance[12]. Previous studies on MOF-5 ($Zn_4O(BDC)_6$) have demonstrated the semiconductor behvior of this MOF which is one of the first used MOFs as photocatalysts[1,13]. In fact, the organic linkers, excited under irradiation, activate the MOFs metal clusters considered as inorganic semiconductors via linker-to-metal cluster charge transfer (LCCT)[13]. Previous studies on the photoluminiscence of MOF-5 have also cofirmed the possibility of this matrial to act like photocatalyst[1]. Since then, several MOFs based chrominium, titanium, aluminium and zirconium were applied in the photocatalytic field[14,15].

Thanks to the large earth abundance and the low-cost of the iron, Fe-based MOFS became one of the most interesting and attrative MOFs among those reported in the literature and used as photocatalysts[14,16]. Moreover, owing to the presence of the Fe-O cluster, the iron based MOFs exhibit high absorption in visible region which make them more promising and advantageous for phototcatalytic applications[14–16]. Examples of their high photocatalytic performances were reported previously by Li et al. who compared the adsorption and degradation of acid orange 7 via the generation of higly reactive radicals from activated persulfate by four different MIL Fe-based MOFs[17]. Liang et al. have also applied the MIL-53(Fe) as photocatalyst for the simultaneous reduction of Cr(IV) and oxidation of organic dyes, methyl orange and rhodmine B under visible light[18].

The different interesting propreties of MOFs including their large surface area, their semiconductor behavior, their low-cost and ease of synthesis have make them very attractive for several applications fields[19]. However, these catalysts are generally synthesized in powder dispersed form with poor chemical stability and processability which limit their catalytic applications where shaped catalysts are generally more desired. Indeed, thanks to their enhanced mechanical properties and their resistance to high applied wastewater flow, immobilized photocatalysts can be recycble and reuse through facile processes, avoiding then supplementary expensive and time-consuming regeneration steps[20–23]. Therefore, immobilizing MOFs into suitable matrix was an interesting solution to overcome these catalysts disadvantages[20]. In this context, Chang et al. have developed a structured SiO_2/MIL-100(Fe) membrane characterized by an important catalytic efficiency for the degradation of Rhodamine B under visible irradiation[20]. Thanks to polymers exceptional properties including chemical and thermal stability as well as their flexibility and good mechanical properties, associating them with MOFs inside or outside their pores, was also a considerable solution to enhance the workability and the processability of these materials[21,24]. Indeed, Zhang et al. have modified the surface of different MOFs by their association with PDMS layer, deposited via a thermal process, ameliorating then the MOFs stability towards water degradation[25]. The same group have also reported the hybridization of UiO-66-NH_2 MOF functionalized by methacrylate anhydride polymerizable functional groups, with butyl methacrlyate under UV light irradiation, obtaining then an elastic membrane with enhanced separation proprties[26].

In this study, we report the successful synthesis of a new Fe-based MOF/polymer composites, by a facile, green and rapid post photopolymerization process, realized at ambient temperature and withtout the release of volatil organic compounds[27]. The obtained shaped hybrid materials gathered the good processability, maellability and robustenss of the polymer as well as the remarkable photocatlytic activities of the MOFs towards the degradation of organic pollutants when exposed to irradiation sources. This strategy facilitated then their applications in the photocatalytic filed where high pollutant flow rate are generally applied at the photocatalysts, and especially their recovering and regeneration avoiding then the time-consuming steps of filtration or centrifugation usually carried out at the end of the photocatalytic process.

The stability, surface structure, porosity, optical and mechanical properties of the developped MOF/polymer photocomposites were fully characterized by several analytical techniques such as Thermogravimetric Analysis (TGA), Transmission Electron Microscopy (TEM), Scanning Electron Microscopy (SEM), Energy-dispersive X-ray analyses (EDX), X- Ray Diffraction analysis (DRX), Fourier-Transform Infrared Spectroscopy (FTIR), BET specific surface area, Dynamic Mechanical Analysis (DMA), Atomic Force Microscopy (AFM) and UV-Visible diffuse reflectance spectroscopy. Furthermore, the newly developped materials exhibit high photocatalytic efficiency for the removal of Acid Black from water under UV lamp irradiation and without the addition of oxidatives chemicals, even after several photocatalytic cycles. Acid Black was targeted as model dye to test the photocatalytic ability of the Fe-based MOF/polymer composites, because of its hamrful impacts in the environment, its cariogenic effects and its massive presence in the texitile industries sewages[28,29]. Degradation routes, were also studied based on different scavenging experiments under air and under N_2. Such applications of MOFs were fewly reported in the litteratue, however these catalysts were generally used as powdred samples, not as immobilized or shaped ones[30].

2. Experimental section

2.1. MOFs synthesis

2.2. Other chemicals compounds

Trimethylolpropane triacrylate (TMPTA from Allnex) was chosen as monomer for composites develeopement. *Bis*(4-*tert*-butylphenyl) iodonium hexafluorophosphate (Iod or Speedcure 938), phenyl *bis*(2,4,6-trimethylbenzoyl) phosphine oxide (BAPO or Speedcure BPO), used together as a photoinitiator system, were obtained from Lambson Ltd (UK). EDTA (Ethylenediaminetetraacetic acid), 2,2,6,6-tetramethyl-1-piperidinyloxy (TEMPO) and Acid Black dye were obtained from Sigma Aldrich. 4-Methoxyphenol (MEHQ) and titanium dioxide (predominantly rutile and anatase) were purchased from Alfa Aesar. Structures of the chemicals used in this paper are represented in Figure 1.

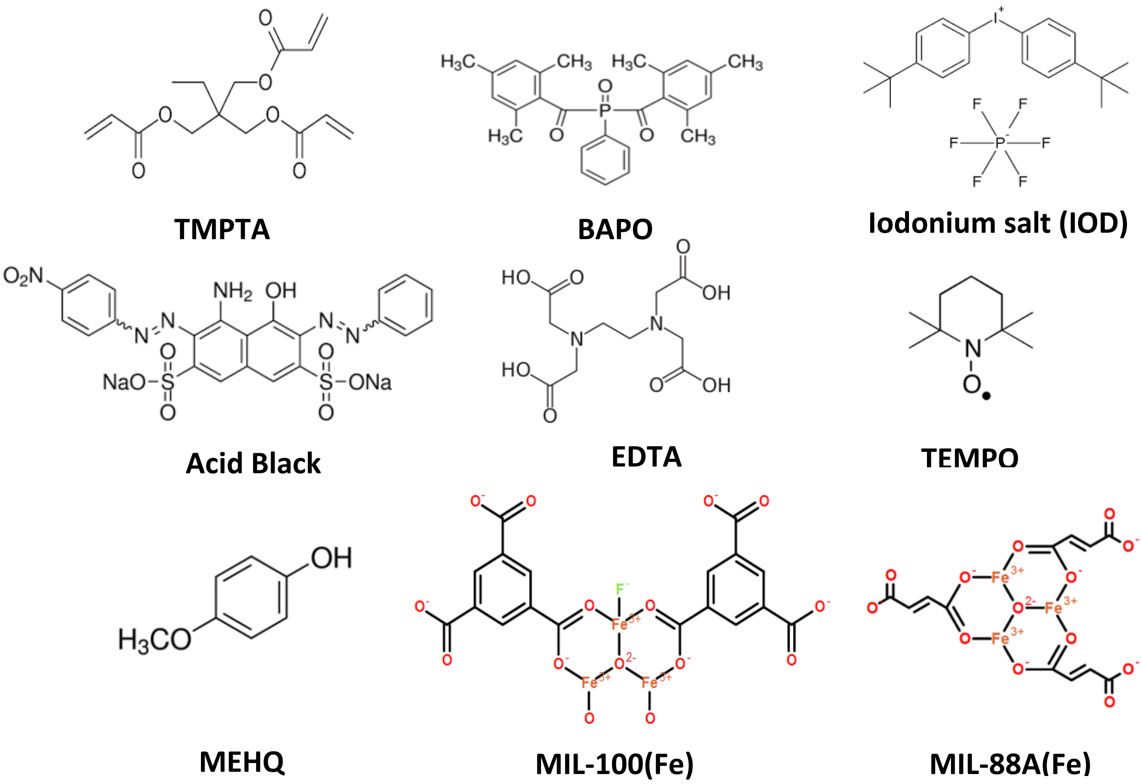

Figure 1. Structures of the chemicals used in this work.

2.3. Photopolymerization experiments

In this study, MIL-100(Fe) and MIL-88A(Fe) MOFs were immobilized in a triacrylate monomer (TMPTA) via a free radical polymerization process, under air and using BAPO and the iodonium salt as a photoinitiator and co-initiator, respectively. The obtained light sensitive resins were placed in a mold to define the final form of the composites (thickness = 1.3 mm), and irradiated by a Light Emitting Diode LED@405 nm (I_0 = 100mW/cm^2). Photopolymerization conversion rates were evaluated by monitoring the gradual change of the TMPTA double bond located at 4730 cm^{-1} for thick samples via a real-time Fourier transform infrared spectroscopy.

2.4. Photocatalytic activity

Photocatalytic efficiency of MIL-100(Fe)/polymer and MIL-88A(Fe)/polymer composites were investigated by Acid Black photodegradation upon an Omnicure Dynamic lamp, series 1000 lumen (I_0 = 250mW/cm^2, λ=320-520nm). The intital concentration and volume of the Acid black were equal to 15mg/L (24.25 µmol/L) and 4ml, respectively, since the photodegradation experiments were carried out directly in the analysis cuvette where the photocomposites pellet were added ih the aqueous solution. pH of the solution was equivalent to 5.9.

The evolution of the model dye concentration was investigated by monitoring its aborbance at 618 nm over time, performed by a JASCO V730 spectrophotometer. The degradation dye rate at different irradiation times was calculated by the following formula (eq.1):

Dye conversion = $(1-\frac{Abs\ t}{Abs\ t=0})$ ×100 (eq.1)

Where $Abs\ t=0$ and $Abs\ t$ are the measured Acid Balck absorbances before and after a given time (t) of irradiation.

2.5. Composites stability

2.5.1. Stability in water

Swelling tests were realized by immersing composites and polymer in water for 24h. The swelling ratio were evaluated using the following formula (eq.2):

Swelling = $(\frac{\mathrm{Ws}}{\mathrm{Wd}}-1)\times 100$ (eq.2)

Where W_d is the initial weight of the material and W_s is the weight of swollen material.

Also, the dry extracts of the different developed materials were calculated after the swelling experiments by drying them in an oven at 50° C for 1h. The dry extract was estimated using the following formula (eq.3):

Dry extract = $\frac{\mathrm{Wsd}}{\mathrm{Wd}}\times 100$ (eq.3)

Where W_{sd} = Weight of dried materials after swelling.

2.5.2. Thermal stability

The Thermogravimetric Analysis (TGA) experiments were carried out by a TGA Mettler Toledo TGA/DSC3+, at temperatures between 30°C to 800 °C, at heating frequency of 10 K/min under a dry airflow of 100 mL/min.

2.6. Composites characterization

2.6.1. Morphological characterization

Morphological characterization was carried out by a JSM-7900F Scanning Electron Microscopy (SEM) from JEOL, possessing an annular detector from DEBEN for transmission images.

2.6.2. Chemical analysis

A QUANTAX double detector from Bruker, was used to realize Energy-dispersive X-ray analyses.

2.6.3. Composites structural characterization

X-ray diffraction experiments were carried out using a Panalytical X'Pert PRO diffractometer equipped with a Cu X-ray tube ($Cu_{K\alpha}$ = 0.1542 nm) operating at 45 kV and 40 mA, and a PIXCel detector.

Fourier transform infrared absorption patterns were obtained in the range of 650–4000 cm^{-1}, by a thermo scientific is-50 FTIR spectrometer, using a diamond golden gate ATR accessory (GRASEBY) from SPECAC.

2.6.4. Composites surface topography and rigidity

Atomic Force Microscopy (AFM) technique was applied for the determination of the roughness and the elastic modulus of the different MOF/polymer composites and the polymer. A Bruker Multimode IV, with a Nanoscope V controller and an E “vertical” scanner (Bruker), and a Peak Force Quantitative Nanomechanical Mapping (PF-QNM, Bruker) method were used for AFM experiments. The concrete experimental spring constant and resonance frequency, equal respectively to 158 N/m and 522,48 KHz were determined thanks to the Sader method. The calibrated Tip radius was equivalent to 75 nm. More details on these characterization technique were reported in our previous works[31].

2.6.5. Textural properties and porosity

Porosities of the different developed materials were evaluated from nitrogen adsorption/desorption at 77.35 K via a micromeritics ASAP 2420 instrument. Standard Brunauer, Emmett, and Teller (BET) method were used to calculate the BET specific surface area and average pore diameter (Gurlich law).

The samples were degassed at 25°C for 60 hours on degassing port and weighted. Then, the samples were degassed once again at 25°C for 4 hours on the analysis port to extract the trapped nitrogen. Analyses were realized with a reactor of the free volume to optimize the measurement and the free volumes were determined after analysis to avoid the pollution of the samples.

2.6.6. Mechanical properties in bulk

Bulk mechanical properties of the synthesized composites were evaluated by a DMA Mettler Toledo DMA861e.

2.6.7. Optical properties

Reflectance measumrements of the polymer as well as the MOF/polymer composites were carried out by UV-visible spectrophotometer (JASCO V-750) equipped with an integrating sphere.

3. Results and discussion

3.1. Synthesis of MOF/polymer composites by photopolymerization

The different Fe-based MOF/polymer composites were synthesized by photopolymerization technique which is the most suitable approach for immobilizing MOFs into polymers. In fact, in contrary to the classical thermal polymerization, no heat was necessary for initiating the polymerization reaction thus avoiding an eventual thermal degradation of MOFs during the synthesis process. The obtained photopolymerization conversion rates for the free radical polymerization (FRP) of TMPTA are reported in Figure 2.

Figure 2 (A), represents the TMPTA polymerization kinetics under visible irradiation in the presence of MOF MIL-100(Fe) with different mass percentages. In fact, it is obvious that the polymerization performance decreases (the final acrylate function conversions (AFC)) by adding the MOF to the initial TMPTA resin containing BAPO as the photoinitiator and the iodonium salt as the co-initiator. The results showed that the acrylate function double bond (C=C) final percentage conversion reached in 60 seconds decreases from 82% to 72%, 68% and 53% in the presence of 0.5%, 1% and 2% of MIL-100(Fe), respectively. This could be explained by the inhibition of light penetration by the incorporated catalyst. Indeed, by increasing the mass percentage of MOF, the prepared formulations become less homogeneous and darker in color, acting in turn as in ternal filter.

Similarly, in the case of MIL-88A(Fe)/polymer composite (Figure 2(B)), the encapsulation of this MOF into the polymer matrix affected the final acrylate function conversions and the polymerization kinetics, especially for the 2%MIL-88A(Fe)/polymer composite. In fact, by reaching this mass percentage, the prepared solution became less homogenous and more pigmented in color which provoked a decrease in the polymerization kinetics and in the final acrylate function conversion from 82% to 40% due to a reduced light penetration within the samples (Figure 2 (B) (4)).

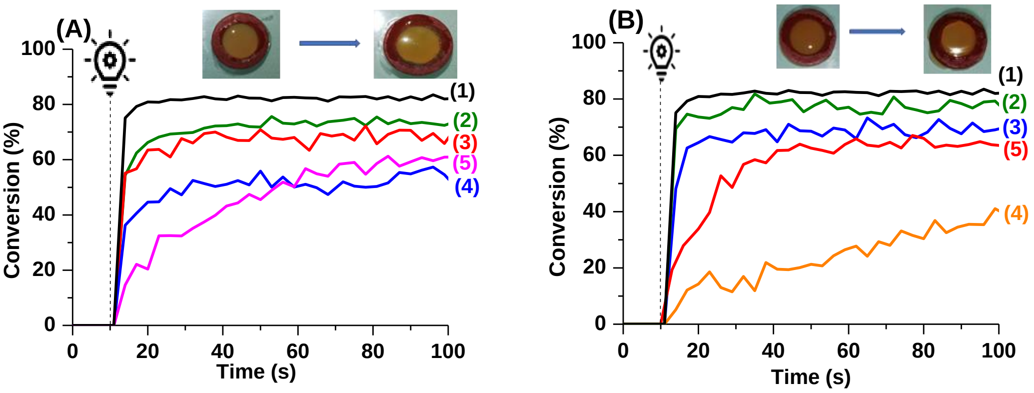

Figure 2. Photopolymerization profiles of acrylate functions (double bond conversion vs irradiation time) under air upon exposure to a LED@405 nm (A) in the presence of BAPO/Iod/MIL-100(Fe) (1) (0.2%/1%/0% (w/w/w)), (2) (0.2%/1%/0.5% (w/w/w)), (3) (0.2%/1%/1% (w/w/w)), (4) (0.2%/1%/2% (w/w/w)), (5) (0.2%/0%/1% (w/w/w)); (B) in the presence of BAPO/Iod/MIL-88A(Fe) (1) (0.2%/1%/0 (w/w/w)), (2) (0.2%/1%/0.5% (w/w/w)), (3) (0.2%/1%/1% (w/w/w)), (4) (0.2%/1%/2% (w/w/w)) and (5) (0.2%/0%/1% (w/w/w)); thickness = 1.3mm; the irradiation starts at t = 10 s.

Figure 2 ((A, B), curves (3 and 5)) show that the addition of the Iodonium salt as the co-initiator for MIL-100(Fe)/polymer and MIL-88A(Fe)/polymer composites synthesis accelerated the polymerization kinetics and increased the final monomer conversions. In fact, in the absence of this chemical, the acrylate function double bond (C=C) final conversion rate reached within 100 seconds was decreased from 67% to 61% and from 68% to 63% in the case of the 1%MIL-100(Fe)/polymer and MIL-88A(Fe)/polymer composites.

Addition of the iodonium salt in the formulations was carried out in order to be able to compare under the same conditions, the current results with those obtained in our previous works on POMs/polymer composites where the presence of this co-initiator had significantly improved the photopolymerization rates as well as the materials photocatalytic efficiency[32].

3.2. MOF/Polymer composite stability

The stability in solutions and at high temperatures of the polymer as well as the synthesized phtotocomposites were investigated in order to improve their photocatalytic applications in the industrial field.

3.2.1. Stability in water

Heterogenous photocatalysis treatements are usually carried out in water, avoinding then the use of supplementary chemicals. Photocatalysts should be therefore, stable in this solvent. Consequently, swelling and dry extract ratios of the synthesized photocomposites were calculated to evaluate their stabilities and the monomer loss probability after polymerization.

Table 1. Acrylates Final Conversion (AFC %), Swelling (%) (in water) and dry extract (%) of different synthesized MOF/polymer composites.

	AFC (%)	Swelling (%)	Dry extract (%)
Polymer	82	10 ± 0.02	100 ± 2
0.5% MIL-100(Fe)/polymer	79	0 ± 0.02	100 ± 2
1% MIL-100(Fe)/polymer	79	0 ± 0.02	100 ± 2
2% MIL-100(Fe)/polymer	80	0 ± 0.02	100 ± 2
0.5% MIL-88A(Fe)/polymer	80	0 ± 0.02	100 ± 2
1% MIL-88A(Fe)/polymer	77	0 ± 0.02	100 ± 2
2% MIL-88A(Fe)/polymer	71	0 ± 0.02	100 ± 2

The very low calculated swelling percentages as well as the large dry extract percentages, reported in Table 1 suggest respectively a highly crosslinked acrylate network despite the MOFs presence into the polymer and a low probability of monomer loss after the polymerization process. This is was line with the obtained high final Acrylates Final Conversion (AFC) proving then the excellent stability of the developed MOF/polymer composites in water.

3.2.2. Thermal stability

Thermal stability of the developed MOF/polymer composites was studied by TGA analysis. DTG curves for the crystallite MOF, the MOF/polymer composites as well as the polymer are shown in Figure 3. The different degradation temperatures are gathered in Table 2.

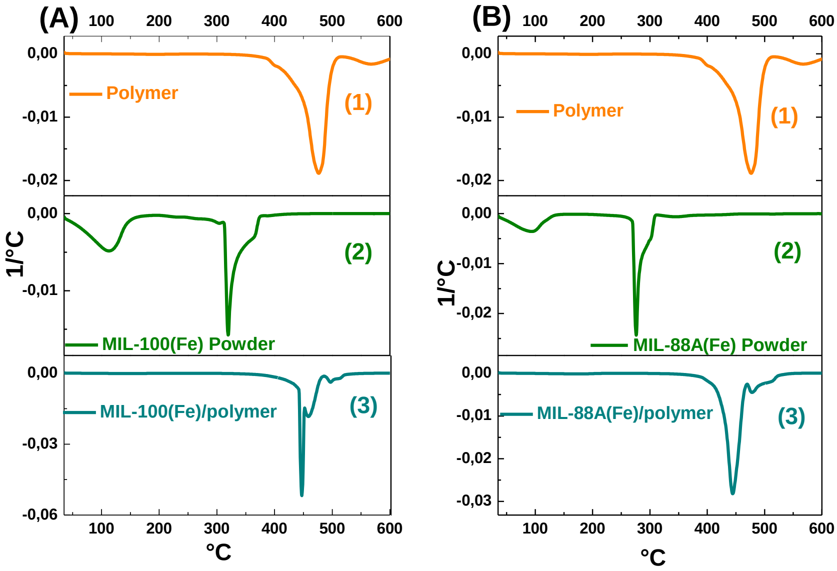

Figure 3. DTG curves of (A) (1) Polymer; (2) MIL-100(Fe) powder and (3) 2% MIL-100(Fe)/polymer composite. (B) (1) Polymer; (2) MIL-88A(Fe) powder and (3)1% MIL-88A(Fe) /polymer composite.

The decomposition temperature of the polymer was slightly decreased by adding the MIL-100(Fe) and the MIL-88A(Fe) MOFs to the initial resin (476 °C for the polymer vs. 446 °C and 444°C for the composites). However, the developed photocatalysts still have high and stable degradation temperatures for the different synthesized materials which promotes their application in the photocatalytic industrial field.

Table 2. Decomposition temperatures of the polymers, the crystals MOFs and the MOF (2% and 1%)/polymer composites.

Material	Polymer	MOF Powder		MOF/polymer composites	
		MIL-100(Fe)	MIL-88A(Fe)	2% MIL-100(Fe)	1% MIL-88A(Fe)
Decomposition temperature(°C)	476	321	378	446	444

3.3. MOF/polymer composites characterization

A full characterization of the as-prepared Fe-based MOF/polymer composites including: morphological, structural, mechanical and optical characterizations, ensures a further understanding of the properties as well as the behavior of these materials as photocatalysts which guarantee a better application performances for intended use in industry.

3.3.1. Morphological and chemical characterization

Taking into account, that heterogenous photocatalysis is a phenomenon occurring at the photocatalyst surface, the developed MOF/polymer composites morphologies were characterized by Scanning Electron Microscopy (SEM) and Transmission Electron Microscopy (TEM). SEM images of the polymer used as a matrix for MOFs incorporation show a homogenous surface for the polymer film (See Figure 4 (a)).

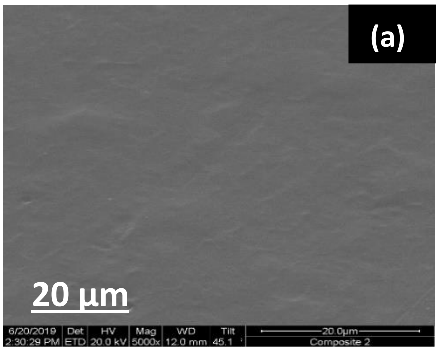

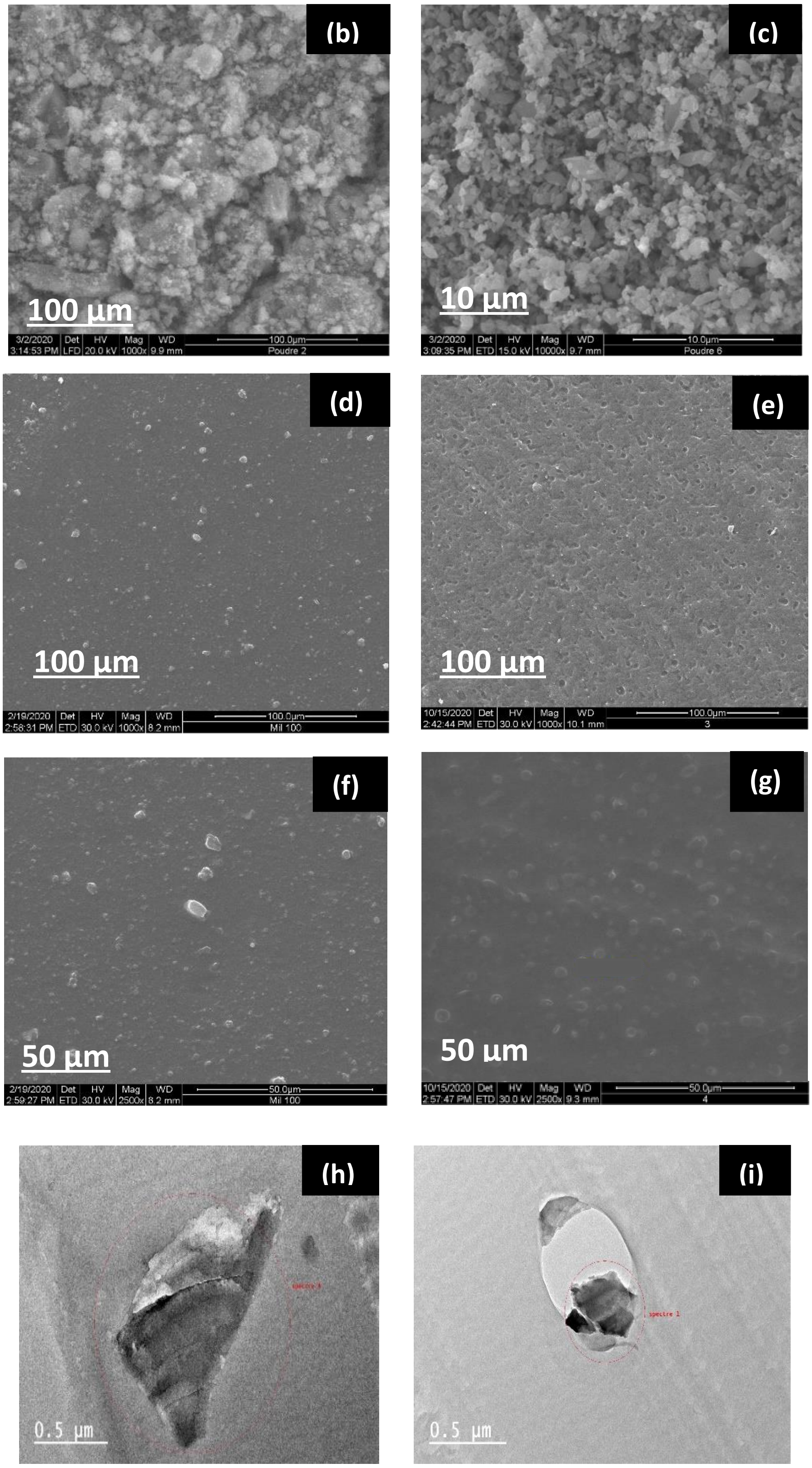

Figure 4. SEM images of (a) polymer without MOF; (b) MIL-100(Fe) powder; (d, f) 2% MIL-100(Fe)/polymer composite at different scales; (c) MIL-88A(Fe) powder; (e, g) 1% MIL-88A(Fe) /polymer composite at different scales. TEM images of (h) 2% MIL-100(Fe)/polymer composite; (i) 1% MIL-88A(Fe) /polymer composite.

It can be clearly seen from the SEM images (Figure 4(b–c)) that the two MOFs displayed different microcrystals. MIL-100(Fe) was principally constituted of irregular flaky-like crystals[33] however, MIL-88A(Fe) presents spindle-like shape crystals[34]. Figure 4 (d, e, f, g) represent the heterogenous surfaces of the MIL-100(Fe)/polymer composite and the MIL-88A(Fe)/polymer composite constituted by a randomly dispersed spherical MOFs aggregates of different sizes varying between 10 nm and 6 µm. Also, Figure 4 (h, i) show TEM images of the MIL-100(Fe)/polymer and MIL-88A(Fe)/polymer composites indicating the presence of these catalysts at the polymer surface.

Moreover, Energy Dispersive X-ray (EDX) analysis was carried out in order to further understand MOFs dispersion at the surfaces of the synthesized composites and to confirm the immobilization of these catalysts into the polymer (See Figure 5).

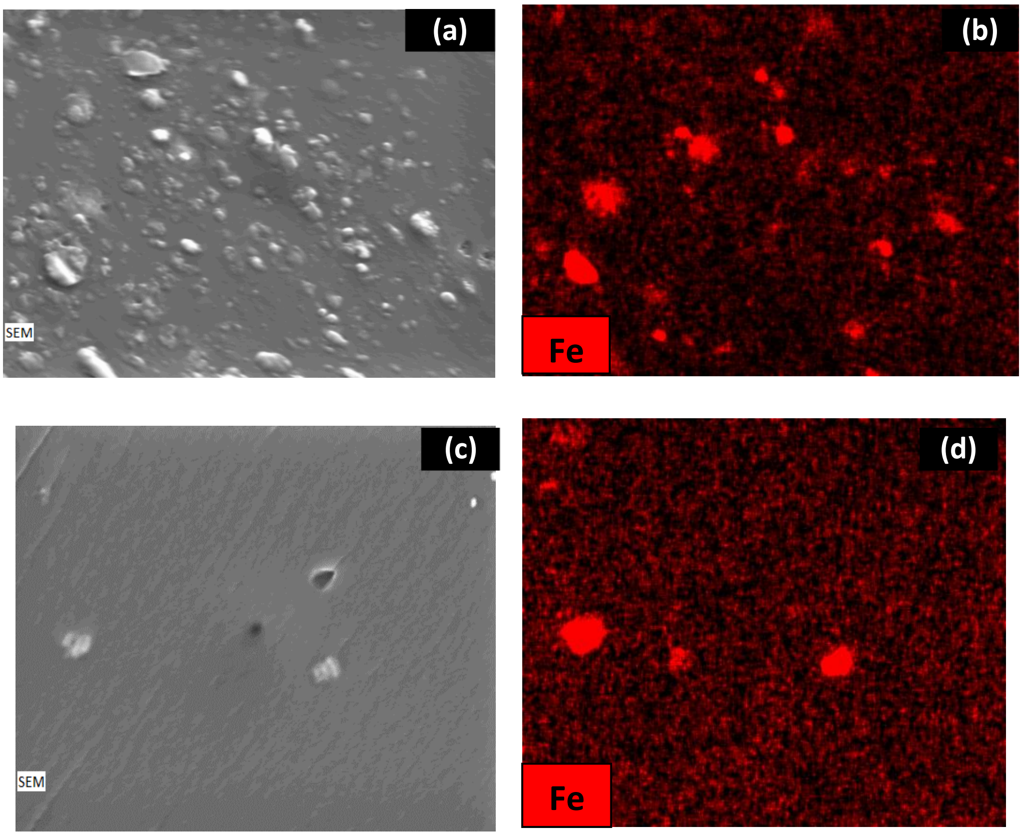

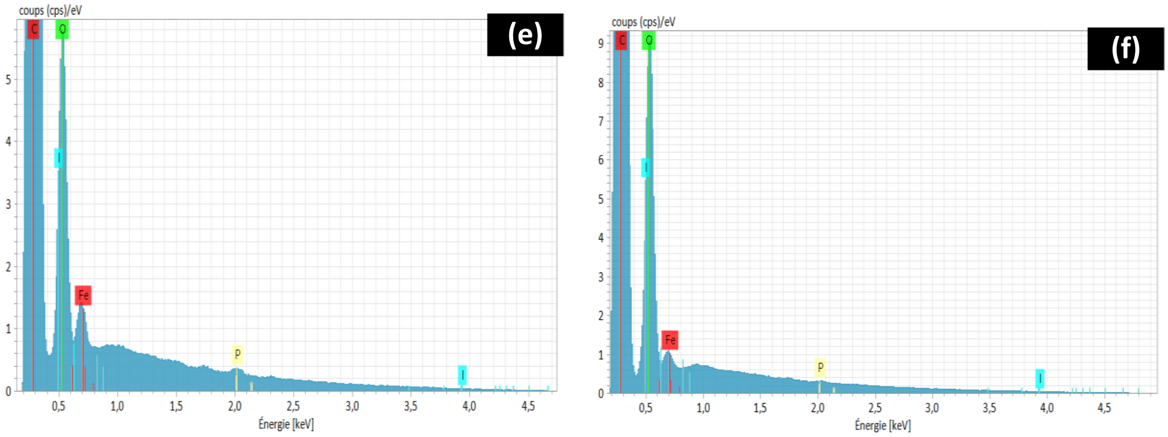

Figure 5. SEM-EDX analysis of (a, b, e) 2% MIL-100(Fe)/polymer composite; (c, d, f) 1% MIL-88A(Fe)/polymer composite.

MEB-EDX mapping results (Figure 5(a, b, c and d)) showed an heterogenous MIL-100(Fe) and MIL-88A(Fe) distribution into the polymer which is in agreement with the obtained SEM images (Figure 4). Furthermore, EDX spectrums (shown in Figure 5(e, f)) confirm also the presence in the composite of iron ions belonging to MOFs, iodonium and phosphorus emerging from the BPO and the iodonium salt used as photoinitiator system during the photopolymerization process, as well as carbon and oxygen coming from TMPTA monomer and the photocatalyst.

In conclusion, TEM, SEM and EDX experiments demonstrate that MOFs are clearly well incorporated into the polymer matrix by photopolymerization which is a mild process.

3.3.2. Structural characterization

In order to confirm the MOFs immobilization into the polymer matrix, the different prepared composites were structurally characterized by FTIR spectroscopy and by X-Ray Diffraction.

3.3.2.1. Fourier-transform infrared spectroscopy

In order to further verify the stability of the MOFs structure after their immobilization into the polymer, Fourier-transform infrared (FTIR) spectra of MOFs, composites and polymer were acquired in the 600–4500 cm^{-1} region and the different spectra. Results are shown in Figure 6, Table 3.

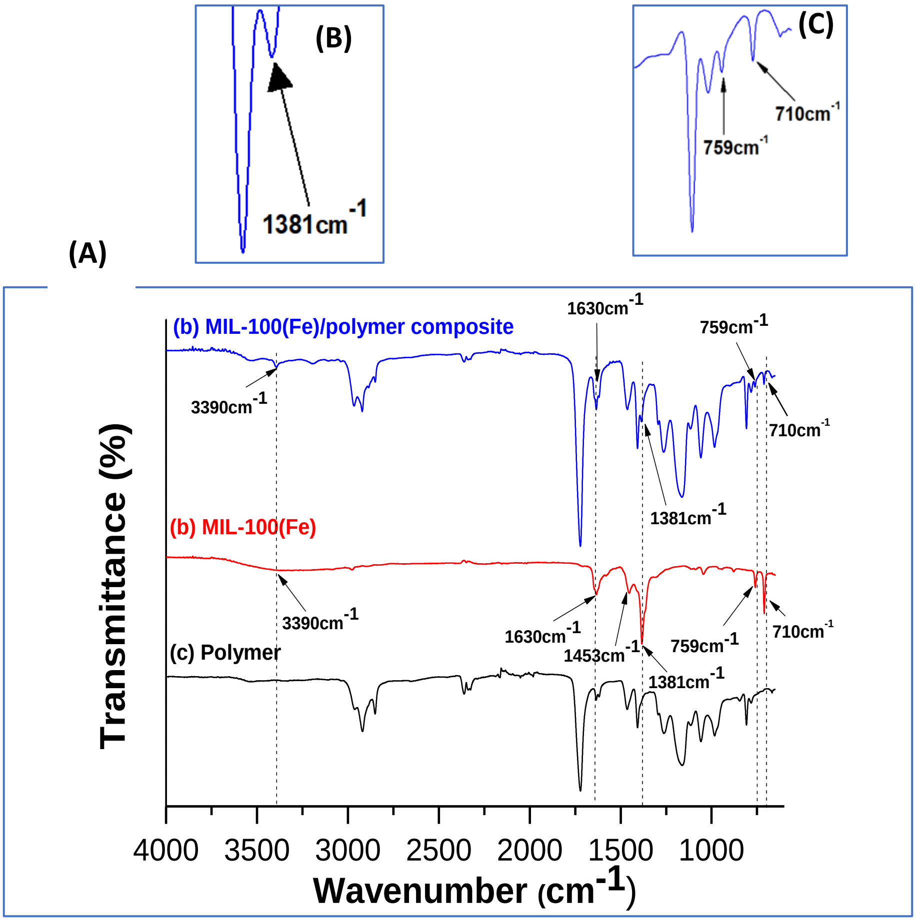

Figure 6. (A) FTIR spectra of (a) the 2% MIL-100((Fe)/polymer composite, (b) the crystalline MIL-100(Fe), (c) the polymer and (B) Zoom-in of 1381 cm^{-1} peak, (C) Zoom-in of 710 cm^{-1} and 759 cm^{-1} peaks.

Table 3. FTIR characterization of the MOF MIL-100(Fe).

	-OH stretching vibration	C=O stretching vibration	C-O symmetric stretching vibration	C-O asymmetric stretching vibration	C-H stretching/Vibration of the benzene ring
Wavenumber (cm-1)	3390	1630	1453	1381	759/710

MIL-100(Fe), MIL-100(Fe)/polymer composite functional groups were studied by FTIR spectroscopy in the range of 4500cm-1 to 600 cm^{-1} (Figure 6, Table 3). The IR spectrum of MIL-100(Fe) shows clear absorption at 3390, 1630, 1453, 1381, 759 and 710 cm^{-1}.The weak curvature at 3369 cm^{-1} is assigned to $^{-}$OH. The peak at 1630 is attributed to v(C=O) of carboxylate group, whereas bands at 1453 and 1381 reflect the symmetric and asymmetric vibrational bands characteristic of the O-C-O group respectively. Also, peaks at 759 and 710 cm^{-1} corresponds to C–H bending vibrations of benzene ring. These identified functional groups of the MIL-100(Fe) are matching with those reported in the literature[35,36]. The FTIR spectrum obtained after incorporating this photocatalyst into the polymer matrix shows five absorptions bands at 3390, 1630, 1381 and 710 and 759 cm^{-1} among the six peaks present in the FTIR spectra of MIL-100(Fe). The non-identification of the last one located at 1453 cm^{-1} could be explained by the low mass percentage of MOF in the polymer matrix which is about 2% or by their superimposition with the polymer intense peaks.

In the case of the MIL-88A(Fe)/polymer composite, the chracteristics peaks of the MOF couldn’t be distinguished from those of the polymer because of its low mass percentage (1%) in the polymer. Increasing the catalyst mass percentage in the TMPTA matrix wass impossible due to the decreasing of polymerization rate (See Figure 2 (B)).

3.3.2.2. X-Ray Diffraction (XRD)

XRD analyses were carried out in order to deeply analyze the molecular structure of composites and to get further insight on the structural variations of the catalyst after its incorporation n into the polymer matrix (See Figure 7).

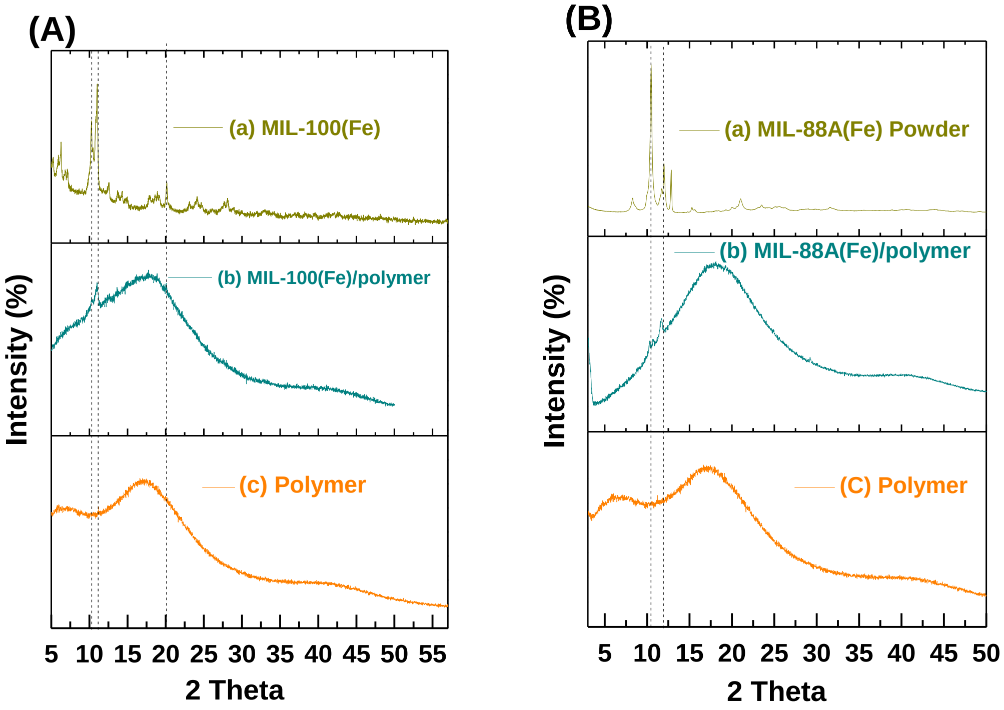

Figure 7. XRD analysis of (A) (a) MIL-100(Fe), (b) 2%MIL-100(Fe)/polymer composite, (c) Polymer and (B) (a) MIL-88A(Fe), (b) 1% MIL-88A(Fe)/polymer composite, (c) Polymer.

The XRD diffraction pattern of the crystallite MIL-100(Fe) (as shown in Figure 7 (A(a)) exhibits different intensive peaks at: 5.26°, 6.06°, 6.32°, 6.85°, 7.11°, 10.38°, 11.03°, 12,57°, 14.22°, 20.14°, 24.11°. These sharp and intense patterns, in line with those previously reported in the literature, indicate a highly crystalline nature of MIL-100(Fe)[35,37,38].

Furthermore, the crystallographic structure of MIL-88A(Fe) was examined by XRD. As seen in Figure 7 (B(a)), the XRD pattern of this MOF shows intense peaks at 2 Theta values of 10.5° and 11.9° already reported in the literature[12,39].

Due to the low mass percentages of these MOFs in the polymer (2% and 1% w/w), their characteristics XRD peaks were hardly identified in the XRD patterns of their corresponding composites because of the decrease of their intensities (Figure 7 (A, B (2)). In fact, only the most intense peaks of the MIL-100(Fe) and the MIL-88A(Fe) located at 2 Theta 10.38°, 11.03° and of the MIL-88A(Fe) situated at 11.9° are also identified, respectively in the XRD patterns in the MIL-100(Fe)/polymer and MIL-88A(Fe)/polymer composites indicating perhaps no crystallinity changes during the photopolymerization process.

3.3.3. Surface properties and porosity

3.3.3.1. BET analysis

To further understand the composites catalysis behavior, it was interesting to estimate their BET surfaces area, the adsorption average pore width and the total area in pores of the different synthesized MOF/polymer composites. Results are gathered in Table 4.

Table 4. BET surface area and adsorption average pore width of the different MOF/polymer based TMPTA composites and of the neat polymer.

	BET surface area ($m^2.g^{-1}$)	Adsorption average pore width (nm)	Total area in pores ($m^2.g^{-1}$)
TMPTA polymer	9.3 ± 0.4	4.3	6.3
0.5% MIL-100(Fe)/polymer	8.8 ± 0.5	4.5	2.3

1% MIL-100(Fe)/polymer	3.4 ± 0.3	7.6	0.8
2% MIL-100(Fe)/polymer	5.5 ± 0.1	4.2	1.9
0.5% MIL-88A(Fe)/polymer	8.3 ± 1.4	2.4	1.6
1% MIL-88A(Fe)/polymer	4.23 ± 0.5	7.3	0.9

The pore size distribution of the neat polymer exhibiting a BET surface area of 9.3 m^2.g^{-1} was already reported in our previous work[31]. This value was decreased by the incorporation of the photocatalysts into the polymer, which could be explained by a probable confinement with the polymer channel[31]. Indeed, the Fe-based MOFs/polymer composites displayed low BET surface areaand total area in pores ranging from 3.4 m^2.g^{-1} to 8.8 m^2.g^{-1} and from 0.8 m^2.g^{-1} to 6.3 m^2.g^{-1}, respectively. The target Fe-MOFs applied as photocatalysts, are immobilized in the polymer whitout degassing and at ambient temperature. In this experimental conditions, the MOFs are in non active and non-porous forms which justify the obtained low BET surface area of the Fe-based MOFs/polymer composites. Improving BET surface area of the developed materials is an objective which will be studied soon in our group.

3.3.3.2. Surface topography by AFM

Roughness and topography of MIL-100(Fe)/polymer composite, MIL-88A(Fe)/polymer composite and the TMPTA neat polymer were characterized by Atomic Force Microscopy (AFM) with the Peak-Force QNM imaging (Figure 8).

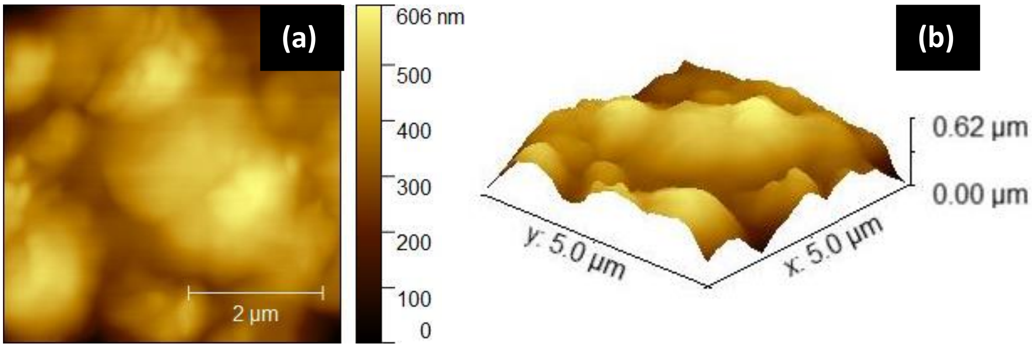

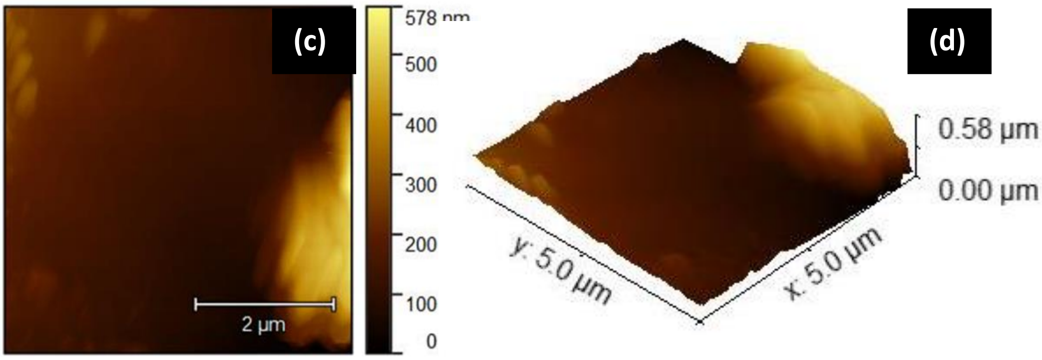

Figure 8. AFM topography images of (a, b) the 1% MIL-100(Fe)/polymer composite and (c, d) the 1% MIL-88A(Fe)/polymer composite.

The neat polymer exhibits a rough surface with a roughness average value (R_a)of 5 nm, already evaluated in our previous works[31]. This surface property was increased to 272 nm and 189 nm by the encapsulation of MIL-100(Fe) and MIL-88A(Fe), respectively into the TMPTA polymer (See Figure 8). The observed difference of roughness between the polymer and MOF/polymer composites is undoubtedly due to the presence of these MOFs at the polymer surface (see EDX data (Figure 5)). Indeed, as shown in Figure 8 (a) which corresponds to a 2D image recorded over an area of 5 µm × 5 µm of the MIL-100(Fe)/polymer composite and in agreement with the SEM images shown in Figure 4, MIL-100(Fe) in the form of cylindric aggregates, is randomly dispersed at the polymer surface. Figure 8 (c) shows also the presence of MIL-88A(Fe) aggregates at the composite surface.

For a facile collect and reuse during the photocatalytic process, photocatalysts should be characterized by a good mechanical's properties. Therefore, effect of the encapsulation of MOFs into the TMPTA neat polymer, on the mechanical properties was investigated.

3.3.4. Mechanical properties

Mechanical properties of the synthesized composites were studied by AFM (Peak-Force QNM imaging mode). Figure 9 shows the recorded topography of the elastic modulus on the surface of the MIL-100(Fe)/polymer and MIL-88A(Fe)/polymer composites.

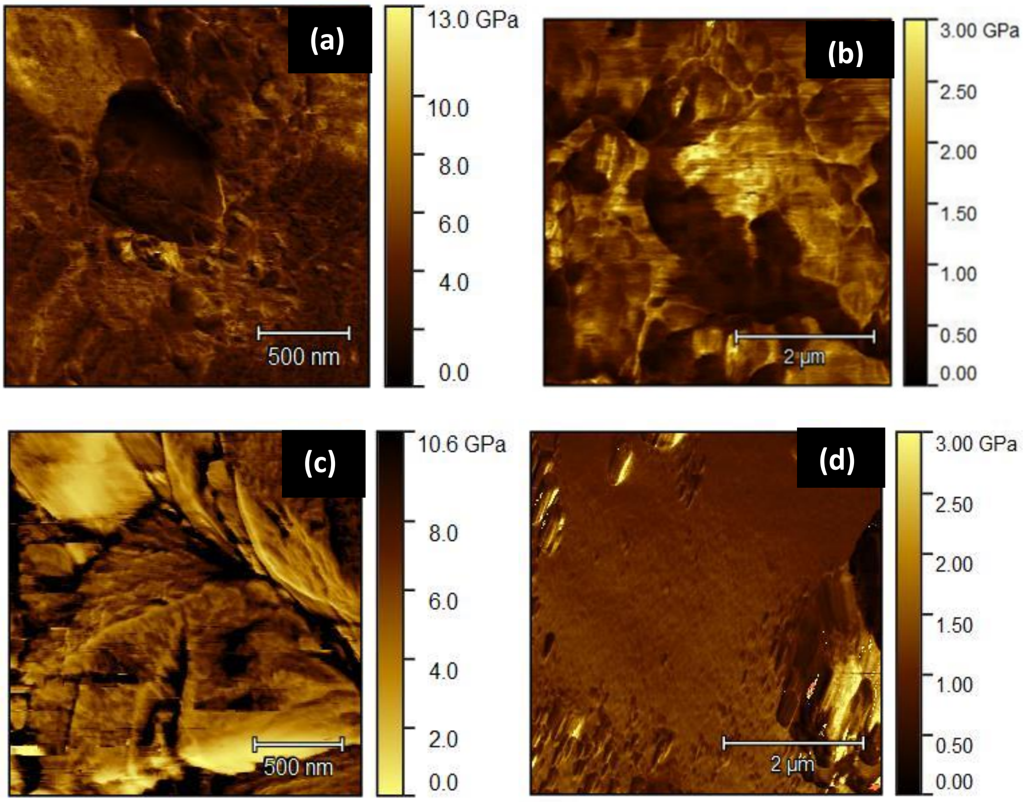

Figure 9. 2D elastic modulus maps (a, b) 1% MIL-100(Fe)/polymer composite and (c, d) 1% MIL-88A(Fe)/polymer composite recorded at different scales.

The elastic modulus distribution of the neat polymer with a mean value of 1.4 GPa was reported in our previous work[31]. This material stiffness was affected by the incorporation of the MOFs based iron. Indeed, MIL-100(Fe)/polymer and MIL-88A(Fe)/polymer composites exhibit mean elastic modulus values of 1.5 GPa and 2.4 GPa, respectively. This change of polymers rigidity is attributed to the MOFs crystals presence at the polymer network surface (See Figure 8 and 9).

Additionally, to the mechanical surface property characterized by AFM, bulk mechanical properties of the composites were evaluated by Dynamic Mechanical Analysis (DMA) experiments. The obtained values of dynamic storage modulus G' and dynamic loss modulus G'' at 25°C are presented in Table 5.

Table 5. Dynamic storage modulus (G'), dynamic loss modulus (G'') at 25°C and Elastic Modulus of TMPTA based polymer, 1% MIL-100(Fe)/polymer and 1% MIL-88A(Fe)/polymer composites.

Composition	Dynamic storage modulus G’(MPa)	Dynamic loss modulus G’’ (MPa)
Polymer	100	20
1% MIL-100(Fe)/polymer	139	13
1% MIL-88A(Fe)/polymer	70	6.5

Based on the results gathered in Table 5, both polymer and MOF/polymer composites exhibit dynamic storage modulus G’ greater than the dynamic loss modulus G’’, proving their rigid characters which is in line with the low swelling degree and the high crosslinking density of the polymer network (Table 1). In bulk, G’ was increased from 100 to 139 by MIL-100(Fe) crystals incorporation into the polymer matrix, improving then its mechanical bulk resistance. However, in the case of MIL-88A(Fe) encapsulation, the dynamic storage modulus of the neat polymer was decreased to 70 MPa, deteriorating then the initial matrix mechanical resistance.

Additionally, G’’ decreases to 13 MPa and 6.5 MPa in the case of MIL-100(Fe)/polymer and MIL-88A(Fe)/polymer composites compared to 20 MPa for the polymer, indicating then a more elastic behavior compared to the initial neat TMPTA polymer. This could be explained by a decrease in the polymer chains mobility and then in the stress transfer in the matrix, by the addition of MOFs crystallites.

Furthermore, since the synthesized MOF/polymer composites will be essentially used for the photodegradation of organic pollutants, their optical properties should be evaluated in order to optimize their photocatalytic activities by choosing the most adequate source of irradiation.

3.3.5. Optical properties

In order to select the most suitable irradiation source for photocatalytic tests, band gap energies of the different MOF/polymer composites were calculated through UV-visible diffuse reflectance spectra and the results are shown in Figure 10 and in Table 6.

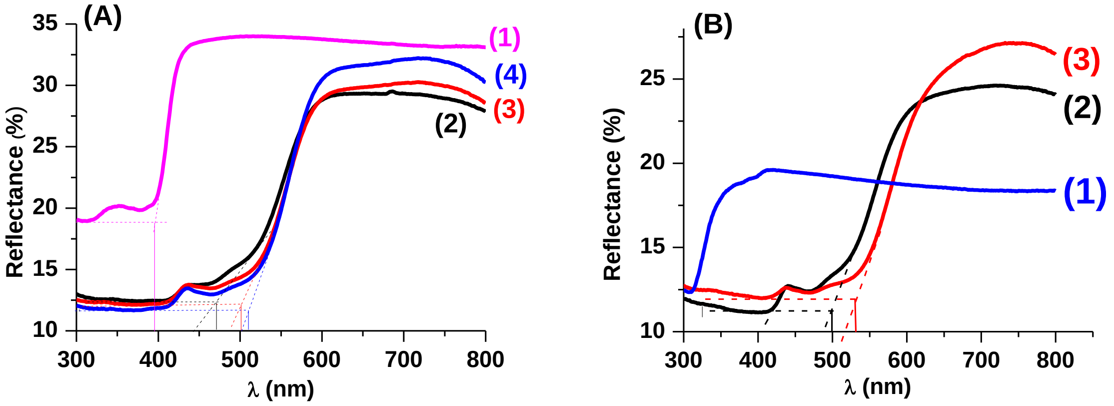

Figure 10. UV-Visible diffuse reflectance spectra of (A) (1) 1% TiO_2/polymer composite, (2) 0.5%, (3) 1%, (4) 2% MIL-100(Fe)/polymer composites and (B) (1) the polymer, (2) 0.5% and (3) 1% MIL-88A(Fe)/polymer composites.

Table 6. Bandgap energy values and absorption wavelengths of different synthesized composites with polymer derived from TMPTA.

	Band Gap energy (eV)	⍰$_{(max)}$ (nm)
Neat polymer	-	-
1% TiO_2/polymer	3.1	396
0.5% MIL-100(Fe)/polymer	2.6	468
1% MIL-100(Fe)/polymer	2.5	488
2% MIL-100(Fe)/polymer	2.4	503
0.5% MIL-88A(Fe)/polymer	2.4	498
1% MIL-88A(Fe)/polymer	2.3	532

Table 6 shows gap energies and absorption wavelengths of the different synthesized Fe-based MOF/polymer composites, which were compared to those of the titanium dioxide/polymer composite. The MIL-100(Fe)/polymer and MIL-88A(Fe)/polymer composites exhibit a band gap energy between 2.3 and 2.6 eV, weaker than that of the TiO_2/polymer composite (3.1 eV). Consequently, the developed photocatalysts are expected to be more performant under visible light than the usually used one in photocatalysis, the TiO_2.

Furthermore, increasing MOFs mass percentages, causes a slight decrease of MOF/polymer composites energy bandgaps and an increase of their reflectance percentages and therefore probably an improvement in their photocatalytic performances. Effectiveness of these different synthesized materials for Acid Black photodegradation will be compared below.

4. Photocatalytic activity of the Fe-based MOF/polymer composites

Photocatalytic activities of the different synthesized Fe-based MOF/polymer composites were tested by monitoring the Acid Black absorbance recorded by UV-visible spectrometry at different irradiation times under UV lamp irradiation. Results are shown in Figure 11 (A, B). Adsorption performances of the photocomposites were evaluated by kepting in the dark during 1 hour the Acid Black acqueous solutions with the photocatalysts. Almost, no dye absorbance decreasing was noticed. This was in agreement with the low BET surface area of the MOF/polymer composites (See Table 4).

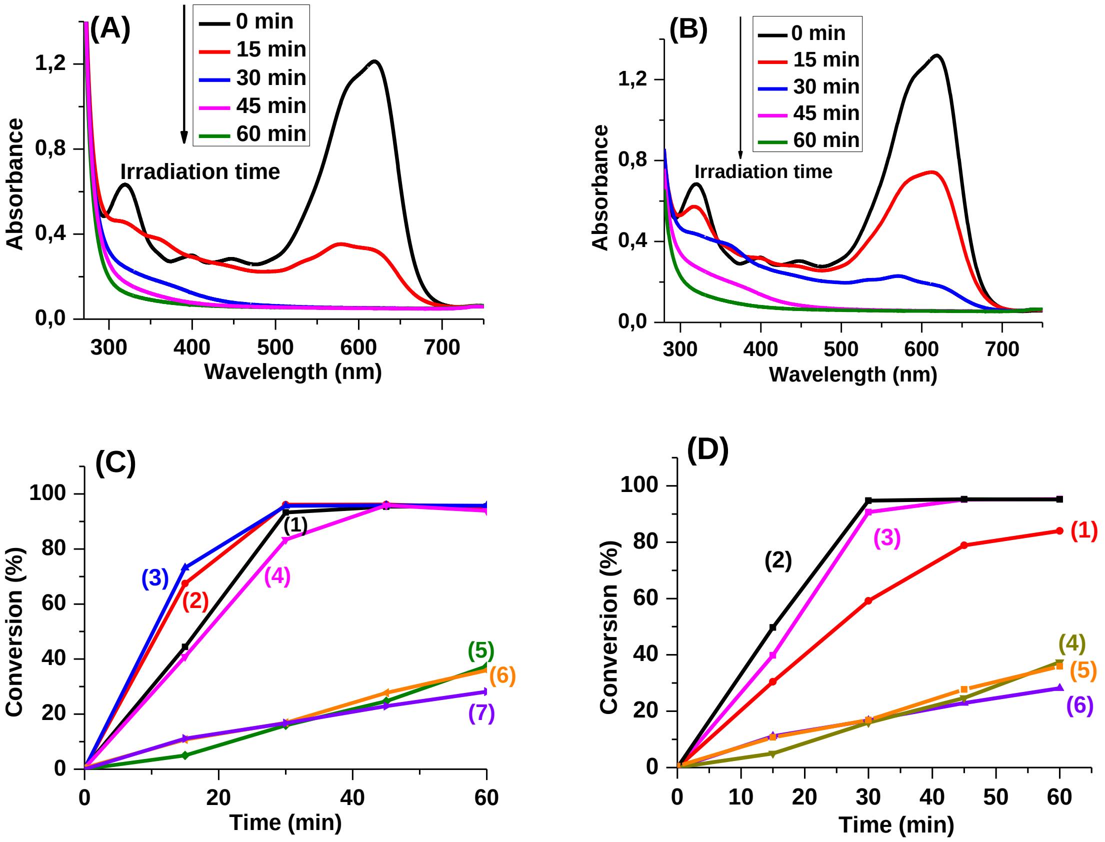

Figure 11. UV-visible absorption spectra of Acid Black water solutions during the photocatalytic degradation process under UV lamp irradiation in the presence of (A) 2% MIL-

100(Fe)/polymer composite and (B) 1% MIL-88A(Fe)/polymer composite. $[AB]_0$ = 15 ppm, pH = 7. Degradation plot of Acid Black (15 ppm) under UV lamp irradiation (C) in the presence of (1) 0.5%, (2) 1%, (3) 2% MIL-100(Fe)/polymer composites, (4) 1% MIL-100(Fe)/polymer composite without iodonium salt, (5) 1%TiO_2/polymer composite, (6) neat polymer, (7) photolysis plot of Acid black without composites and (D) in the presence of (1) 0.5%, (2) 1% MIL-88A(Fe)/polymer composites, (3) 1% MIL-88A(Fe)/polymer without iodonium salt, (4) 1% TiO_2/polymer composite, (5) neat polymer and (6) photolysis plot of Acid black without composites.

Obviously, the two characteristics absorbance peaks of the Acid Black located at 618 nm and 310 nm, corresponding respectively, to the azo group and to the naphtalene transition, decreased gradually during the photocatalytic process in the presence of the MIL-100(Fe)/polymer and the MIL-88A(Fe)/polymer composites (See Figure 11 (A, B)),. This absorbance bands abatement reflects the dye decolorization as well as the degradation of the aromatic part[40,41]. The degradation mechansim of the Acid Black, the possible formation of by-products and the monitoring of the dye solution color changement during the photocatalytic treatment, were discussed in ou previous works (Article MOF 1).

Kinetics of the Acid Blak photodegradation reaction by the two Fe-based MOF/polymer composites as well as their comparaison with the TiO_2/polymer composite and the neat polymer were quantitavely studied by matching the experimental data to the apparent first-order equation given by the following expression[42] :

-Ln(C/C0) = kapp t (1)

Where C_0 and C designate respectively the Acid Black initial concentration and at time t, kapp is the first-order rate constant (min^{-1}) and allows the evaluation of the photocatalytic of the catalyst. Results are shown in Table S_1.

Acid Black concentration is only decreased by 26 % (k_{app}=0.005 min^{-1}) and 35% (k_{app}=0.007 min^{-1}), under 60 min of UV lamp irradiation in the absence of the composites or the polymer and in the presence of the neat polymer, respectively (Figure 11 (C (curves 6, 7)), (D (curves 5, 6))). However 95.2% of this dye is degraded in just 30 min of irradiation in the presence of the Fe-based MOF/polymer composites proving then the remarkable photocatalytic efficiency of the develloped photocomposites which are also more performant than the universal most used photocatalytst, the titanium dioxide. In fact, a commercial TiO_2 encapsulated in the same matrix and under the same experimental conditions than those applied for the synthesis of the MOFs composites, wasn't efficient for the Acid Black degradation. Indeed, under the same time and irradiation source, only 37% (k_{app}=0.007 min^{-1}) was degraded by 1%TiO_2/polymer composite vs. 95% by the 1%MIL-100(Fe)/polymer (k_{app}=0.104 min^{-1}) and the 1%MIL-88A(Fe)/polymer (k_{app}=0.075 min^{-1}) composites (Figure 11 (C (curves 2, 5)), (D (curves 2, 4))).

Remarkably, increasing the mass percentages of crystalline MIL-100(Fe) into the polymer from 0.5% to 1% and 2% and from 0.5% to 1% in the case of crystalline MIL-88A(Fe), enhances respectively, the kinetics of the Acid Black photodegradation from 0.08min^{-1} to 0.104min^{-1} and to 0.108min^{-1} and from 0.03min^{-1} to 0.07min^{-1} (See Table S1 and Figure 11 (C (curves 1, 2, 3), D (curves 1, 2)).

Furthermore, the absence of the Iodonium salt in the polymer matrix which was used as a co-initiator during the photopolymerization process, decreased the kinetics photodegradation from 0.104min^{-1} to 0.059min^{-1} in the case of 1%MIL-100(Fe)/polymer composite, and from 0.075min^{-1} to 0.072min^{-1} in the case of 1%MIL-88A(Fe)/polymer composite (See Table S1 and Figure 11(C (curves 2, 4), D (curves 2, 3))).

Interstingly, the 1%MIL-100(Fe)/polymer composite was more performant for the Acid Black degradation than the 1%MIL-88A(Fe)/polymer composite. In fact, decomposition kinetics calculated for the first photocomposite, equal to 0.104min^{-1}, was higher than that of the second one, equivalent to 0.075min^{-1}. This difference of efficiency could be explained, by the lower fluorescence emission intensity of the first photocomposite compared to that of the second one reflecting therefore, a lower electrons-holes recombination rate[43]. Fluorescence emission spectra of the two developed MOF/polymer composites are reported in Figure 12. The used excitation source emitted at 254 nm wavelength.

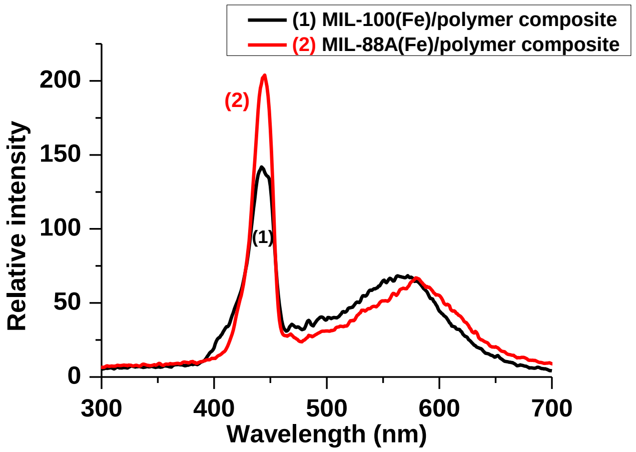

Figure 12. Fluorescence emission spectra of the two different MOF/polymer composites : (1) 1%Mil-100(Fe)/polymer composite, (2) 1%MIL-88A(Fe)/polymer composite.

5. Proposed photocatalytic degradation mechanism

In order to understand the enhanced degradation mechanism of the Acid Black by the newly developed Fe-based MOF/polymer composites, photolysis under different atmospheres (Air and N$_2$) and radical-trapping experiments were carried out. In this study, EDTA[44,45], isopropanol[46], MEHQ[47] and TEMPO[48] were applied as scavengers of h$^+$, Hydroxyl radicals ($^{\bullet}$OH), oxygen active species (RO$^{\bullet}$ and ROO$^{\bullet}$) and carbon centered radicals, respectively. The trappers concentrations were equal to 1Mm and their impacts on the Acid Black photodegradation were identified by monitoring this dye concentration under UV lamp irradiation (See Figure 13).

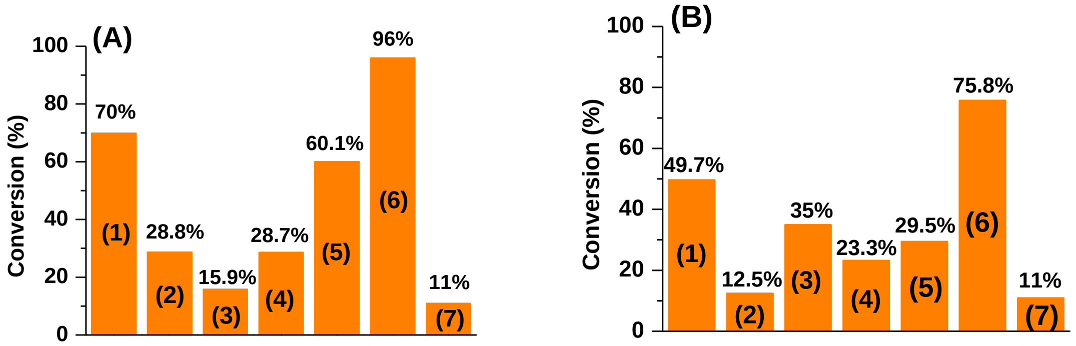

Figure 13. Effects of different scavengers on the degradation of Acid Black under UV lamp irradiation at t=15min, in the presence of (A) 2% MIL-100(Fe)/polymer composite and (B) 1% MIL-88A(Fe)/polymer composite: (1) Without scavengers, under air, (2) Without scavengers,

under N_2. Under air, with the addition of (3) TEMPOL, (4) MEHQ, (5) Isopropyl alcohol and (6) EDTA. (7) Without composite, without scavengers.

Figure 13 (batons 1 and 2) proves the important role played by the dissolved oxygen in the enhancement of Acid Black degradation in the presence of the Fe-based MOF/polymer composites. In fact, under N_2 and under 15 min of UV lamp irradiation, the Acid Black conversion rate was decreased from 70% and 48.7% to 28.8% and 12.6% respectively, in the presence of 2%MIL-100(Fe)/polymer and 1%MIL-88A(Fe)/polymer composites demonstrating the significant function of $^{\bullet}O_2^-$, formed by the reaction between the excited e^- and the O_2 dissolved in the solution, during the photocatalytic process. This was in agreement with the high Acid Black removal rates obtained after adding the EDTA into the aqueous solution. Indeed, conversion percentages were increased from 70% to 96% and from 49.7% to 75.8% in the presence of 2%MIL-100(Fe)/polymer and 1%MIL-88A(Fe)/polymer composites, respectively. The enhancement of the photodegradation process in the presence of this holes scavenger, could be explained by the inhibition of recombination between the excited electons under UV lamp irradiation and the holes through surface and direct recombinations. Therefore, more $^{\bullet}O_2^{-}$ are formed since more migrated electons are present at the composites surface and could react with the dissoved oxygen present in the aqueous solution. Hence, $^{\bullet}O_2^{-}$ are the most important radical species involved in the photodegradation route of the different Fe-based MOFs/polymer composites.

Furthermore, the addition of MEHQ and isopropyl alcohol declined the dye degradation from 70% and 49.7% to 28.7%, 60.1%, and to 23.3%, 29.5% after 15 min of UV lamp irradiation in the presence of MIL-100(Fe)/polymer and MIL-88A(Fe)/polymer composites, respectively (Figure 13 (A and B (batons 1, 4 and 5). The obtained results show the oxygenated active species and the hydroxyl radicals are also implicated in the Acid Black degradation mechanism.

Besides, in the presence of TEMPO, in the Acid Black aqueous solution, the dye degradation was reduced from 70% and 49.7% to 16.9% and 35%, respectively, in the presence of the 2%MIL-100(Fe)/polymer and 1%MIL-88A(Fe)/polymer composites, showing that carbonated radicals participates also in the Acid Black removal route (See Figure 13 (batons 1 and 3).

Based on the trapping experiments above, the degradation mechanism of the Acid Black by the two different Fe-MOF/polymer composites could be explained by the excitation of electrons from the valence band (VB) to the conduction band (CB) and the formation of holes in the VB. This phenomenon occurrs when the composites photocatalysts absorb equivalent or higher energy than their band gap energies. The photogenerated electons migrate to the catalyst surface and reduce the dissolved oxygen in the aqueous solution (O_2) to superoxide radicals ($^{\bullet}O_2^{-}$) which are transformed in their turn to hydroxyl radicals ($^{\bullet}OH$). Simutaneously, holes oxidize water molecules into hydroxyl radicals ($^{\bullet}OH$). Such, decomposition mechanisms, were already reported in the literature by Wang et al. who have applied Fe-MOFs for the adsorption and photodegradation of tetracycline by Fe-based MOFs[14]. C. Das et al. have also demonstrated the same decomposition route, when photodegrading the methyl orange dye by an UTSA-38 MOF[49].

6. Fe-based MOF/Polymer composites reusability and stability study

Recyclabilty and stability of the photocatalysts are ones of the most important parameters for photocatalytic environmental practical applications. To investigate these significant indexes, the photocomposites were recovered from the Acid Black solution, washed with water, dried in air and then used for 10 successive photodegradation cycles. Results are shown in Figure 14.

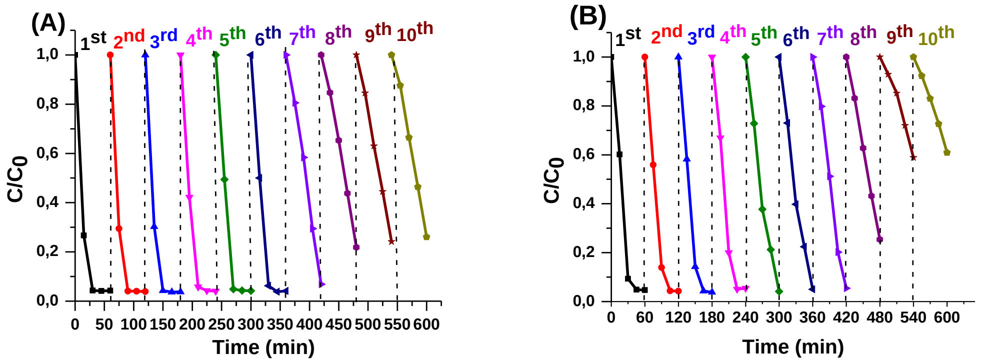

Figure 14. Ten consecutive Acid Black photodegradation cycles over (A) 2% MIL-100(Fe)/polymer composite and (B) 1% MIL-88A(Fe)/polymer composite. $[AB]_0$=15ppm, pH=7, irradiation source: UV Lamp.

Figure 14 shows that the photocatalytic performance of the MIL-100(Fe)/polymer composite starts to decrease from the 7th cycles and from the 5th cycle, in the case of the MIL-88A(Fe)/polymer composite. Indeed, the first photocatalyst still more performant than the neat polymer even after the seventh catalytic cycle and until the tenth process showing its high catalytic stability by a facile and low-cost recovery and regeneration process. However, the second one lose totally its photocatalytic efficiency starting from the ninth cycle. Therefore, these experiments prove the advantages of the immobilization of the MOFs into the polymer consisting in the enhancement of their mechanical properties in order to facilitate their recovery and regeneration. Hence, usually time-consuming and expensive regeneration methods could be avoided.

Photostability of the different developped composites were also investigated by comparing SEM characterizations images before and after the photocatalytic process (See Figure 15).

Figure 15 (a, b) shows, that the MIL-100(Fe)/polymer composite surface wasn’t altered by the irradiation. Approximatively, the same MIL-100(Fe) MOFs density still present at the surface of the polymer after the photodegradation process. However, in the case of the MIL-88A(Fe)/polymer composite less MOFs remain at the surface which could explain the decrease of the photocatalytic activity of this composite starting from the 5th degradation cycle. The better stability of the MIL-100(Fe)/polymer composite during the regeneration and reuse, in comparaison to that of the MIL-88A(Fe)/polymer composite could be probably due to its higher dynamic storage modulus (G’) reflecting a better bulk rigidity (See Table 5).

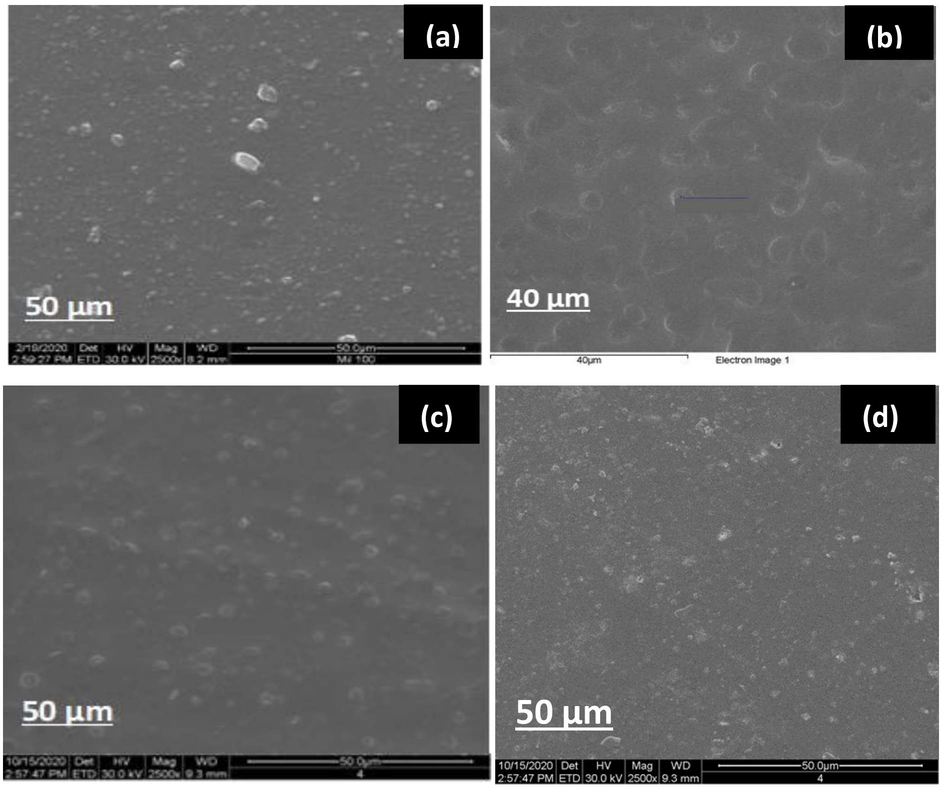

Figure 15. SEM-EDX images of 2% MIL-100(Fe)/polymer composite (a) before and (b) after one photodegradation cycle. SEM-EDX images of 1% MIL-88A(Fe)/polymer composite (c) before and (d) after one photodegradation cycle.

Conclusion

In this study, two Fe-based MOFs/polymer composites with higher photocatalytic properties have been successfully fabricated by a simple, low-cost, rapid and green photopolymerization process under mild visible Light Emitting Diode LED@405 nm irradiation. The developed photocatalysts exhibited exceptional photocatalytic performances, compared to the universal and most used one, the titanium dioxide which was applied in the same experimental conditions than the MOFs/polymer composites. Approximatively, 95% of the Acid Black dye, chosen as poulltant model to evaluate the photocatalytix activities of these photocomposites was removed from water under only 30 minutes of UV lamp irradiation.

Moreover, in order to get futher insight the Acid Black degradation mechanism in the presence of the synthesized MOF/polymer composites, several experiments were realized under different atmospheres and in the presence of three scavangers used separately. Dissolved oxygen seemed to be the key species for Acid Black degradation. Superoxide, hydroxyl, oxygenated and carobonated radicals were also involved in the dye decomposition.

Characterization of the new proposed materials were fully investigated by various methods including XRD, AFM, DMA, SEM, TEM, EDX, FTIR which have verified the fruitful MOFs immobilization into the polymer matrix. The shaped materials displayed enhanced rigidity and high thermal stability, allowing their recovering from the aqueous solution and their reuse by a simple, inexpensive and rapid method. Therefore, the two composites remain photocatlytically actifs under UV lamp irradiation after several degradation process.

In conclusion, associating MOFs with polymers simplified and facilitated their tecnological environemental applications, by obtaining composites gathering at the same time, the processability of the polymer and the interesting photocatalytic activity of the MOFs. This method of synthesis have proved its effectiveness in this work, and could then be used to immobilize a large number of other photocatlysts. Further studies will be carried out in order to improve the polymer stability and to develop composites with larger active surface area.

Table of contents Graphic (TOC)

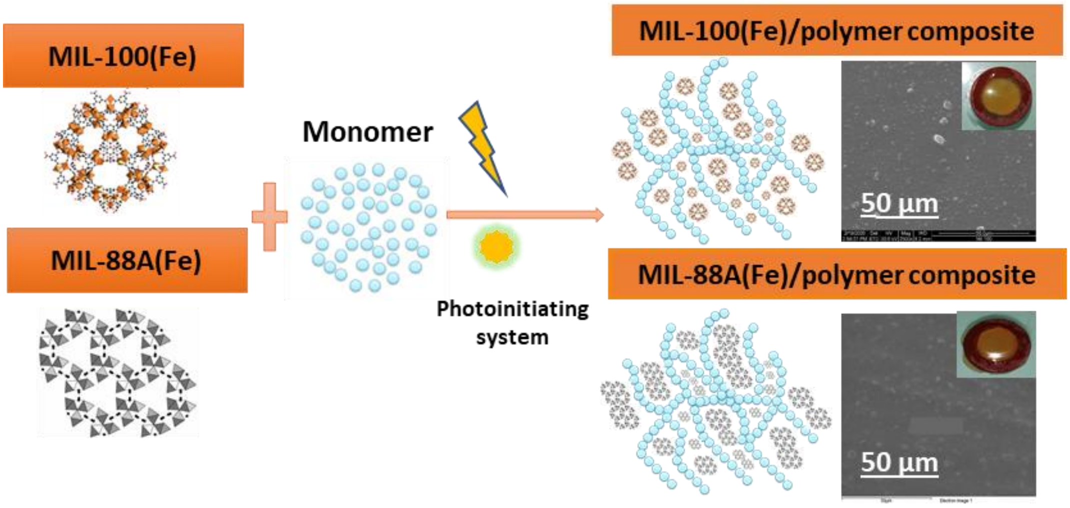

References

(1) Alvaro, M.; Carbonell, E.; Ferrer, B.; Llabrés i Xamena, F. X.; Garcia, H. Semiconductor Behavior of a Metal-Organic Framework (MOF). *Chem. Eur. J.* **2007**, *13* (18), 5106–5112. https://doi.org/10.1002/chem.200601003.

(2) Nasalevich, M. A.; Hendon, C. H.; Santaclara, J. G.; Svane, K.; van der Linden, B.; Veber, S. L.; Fedin, M. V.; Houtepen, A. J.; van der Veen, M. A.; Kapteijn, F.; Walsh, A.; Gascon, J. Electronic Origins of Photocatalytic Activity in D0 Metal Organic Frameworks. *Sci Rep* **2016**, *6* (1), 23676. https://doi.org/10.1038/srep23676.

(3) Carboni, M.; Abney, C. W.; Liu, S.; Lin, W. Highly Porous and Stable Metal–Organic Frameworks for Uranium Extraction. *Chem. Sci.* **2013**, *4* (6), 2396. https://doi.org/10.1039/c3sc50230a.

(4) Tamames-Tabar, C.; García-Márquez, A.; Blanco-Prieto, M. J.; Serre, C.; Horcajada, P. MOFs in Pharmaceutical Technology. In *Bio- and Bioinspired Nanomaterials*; Ruiz-Molina, D., Novio, F., Roscini, C., Eds.; Wiley-VCH Verlag GmbH & Co. KGaA: Weinheim, Germany, **2014**; pp 83–112. https://doi.org/10.1002/9783527675821.ch04.

(5) Li, H.; Wang, K.; Sun, Y.; Lollar, C. T.; Li, J.; Zhou, H.-C. Recent Advances in Gas Storage and Separation Using Metal–Organic Frameworks. *Materials Today* **2018**, *21* (2), 108–121. https://doi.org/10.1016/j.mattod.2017.07.006.

(6) Dong, J.; Zhao, D.; Lu, Y.; Sun, W.-Y. Photoluminescent Metal–Organic Frameworks and Their Application for Sensing Biomolecules. *J. Mater. Chem. A* **2019**, *7* (40), 22744–22767. https://doi.org/10.1039/C9TA07022B.

(7) Dhakshinamoorthy, A.; Li, Z.; Garcia, H. Catalysis and Photocatalysis by Metal Organic Frameworks. *Chem. Soc. Rev.* **2018**, *47* (22), 8134–8172. https://doi.org/10.1039/C8CS00256H.

(8) Wang, C.-C.; Li, J.-R.; Lv, X.-L.; Zhang, Y.-Q.; Guo, G. Photocatalytic Organic Pollutants Degradation in Metal–Organic Frameworks. *Energy Environ. Sci.* **2014**, *7* (9), 2831–2867. https://doi.org/10.1039/C4EE01299B.

(9) Bedia, J.; Muelas-Ramos, V.; Peñas-Garzón, M.; Gómez-Avilés, A.; Rodríguez, J. J.; Belver, C. A Review on the Synthesis and Characterization of Metal Organic Frameworks for Photocatalytic Water Purification. *Catalysts* **2019**, *9* (1), 52. https://doi.org/10.3390/catal9010052.

(10) Gómez-Avilés, A.; Peñas-Garzón, M.; Bedia, J.; Dionysiou, D. D.; Rodríguez, J. J.; Belver, C. Mixed Ti-Zr Metal-Organic-Frameworks for the Photodegradation of Acetaminophen under Solar Irradiation. *Applied Catalysis B: Environmental* **2019**, *253*, 253–262. https://doi.org/10.1016/j.apcatb.2019.04.040.

(11) Wang, C.-C.; Du, X.-D.; Li, J.; Guo, X.-X.; Wang, P.; Zhang, J. Photocatalytic Cr(VI) Reduction in Metal-Organic Frameworks: A Mini-Review. *Applied Catalysis B: Environmental* **2016**, *193*, 198–216. https://doi.org/10.1016/j.apcatb.2016.04.030.

(12) Andrew Lin, K.-Y.; Chang, H.-A.; Hsu, C.-J. Iron-Based Metal Organic Framework, MIL-88A, as a Heterogeneous Persulfate Catalyst for Decolorization of Rhodamine B in Water. *RSC Adv.* **2015**, *5* (41), 32520–32530. https://doi.org/10.1039/C5RA01447F.

(13) Llabrés i Xamena, F. X.; Corma, A.; Garcia, H. Applications for Metal−Organic Frameworks (MOFs) as Quantum Dot Semiconductors. *J. Phys. Chem. C* **2007**, *111* (1), 80–85. https://doi.org/10.1021/jp063600e.

(14) Wang, D.; Jia, F.; Wang, H.; Chen, F.; Fang, Y.; Dong, W.; Zeng, G.; Li, X.; Yang, Q.; Yuan, X. Simultaneously Efficient Adsorption and Photocatalytic Degradation of Tetracycline by Fe-Based MOFs. *Journal of Colloid and Interface Science* **2018**, *519*, 273–284. https://doi.org/10.1016/j.jcis.2018.02.067.

(15) Wang, D.; Albero, J.; García, H.; Li, Z. Visible-Light-Induced Tandem Reaction of o - Aminothiophenols and Alcohols to Benzothiazoles over Fe-Based MOFs: Influence of the Structure Elucidated by Transient Absorption Spectroscopy. *Journal of Catalysis* **2017**, *349*, 156–162. https://doi.org/10.1016/j.jcat.2017.01.014.

(16) Wang, D.; Wang, M.; Li, Z. Fe-Based Metal–Organic Frameworks for Highly Selective Photocatalytic Benzene Hydroxylation to Phenol. *ACS Catal.* **2015**, *5* (11), 6852–6857. https://doi.org/10.1021/acscatal.5b01949.

(17) Li, X.; Guo, W.; Liu, Z.; Wang, R.; Liu, H. Fe-Based MOFs for Efficient Adsorption and Degradation of Acid Orange 7 in Aqueous Solution via Persulfate Activation. *Applied Surface Science* **2016**, *369*, 130–136. https://doi.org/10.1016/j.apsusc.2016.02.037.

(18) Liang, R.; Jing, F.; Shen, L.; Qin, N.; Wu, L. MIL-53(Fe) as a Highly Efficient Bifunctional Photocatalyst for the Simultaneous Reduction of Cr(VI) and Oxidation of Dyes. *Journal of Hazardous Materials* **2015**, *287*, 364–372. https://doi.org/10.1016/j.jhazmat.2015.01.048.

(19) Ahmed, I.; Jhung, S. H. Composites of Metal–Organic Frameworks: Preparation and Application in Adsorption. *Materials Today* **2014**, *17* (3), 136–146. https://doi.org/10.1016/j.mattod.2014.03.002.

(20) Chang, M.-J.; Cui, W.-N.; Chai, X.-J.; Liu, J.; Wang, K.; Qiu, L. Fabrication of Flexible MIL-100(Fe) Supported SiO2 Nanofibrous Membrane for Visible Light Photocatalysis. *J Mater Sci: Mater Electron* **2019**, *30* (2), 1009–1016. https://doi.org/10.1007/s10854-018-0370-9.

(21) Kalaj, M.; Bentz, K. C.; Ayala, S.; Palomba, J. M.; Barcus, K. S.; Katayama, Y.; Cohen, S. M. MOF-Polymer Hybrid Materials: From Simple Composites to Tailored Architectures. *Chem. Rev.* **2020**, *120* (16), 8267–8302. https://doi.org/10.1021/acs.chemrev.9b00575.

(22) Chen, L.; Xu, Q. Metal-Organic Framework Composites for Catalysis. *Matter* **2019**, *1* (1), 57–89. https://doi.org/10.1016/j.matt.2019.05.018.

(23) Hou, L.; Wang, L.; Zhang, N.; Xie, Z.; Dong, D. Polymer Brushes on Metal–Organic Frameworks by UV-Induced Photopolymerization. *Polym. Chem.* **2016**, *7* (37), 5828–5834. https://doi.org/10.1039/C6PY01008C.

(24) Kitao, T.; Zhang, Y.; Kitagawa, S.; Wang, B.; Uemura, T. Hybridization of MOFs and Polymers. *Chem. Soc. Rev.* **2017**, *46* (11), 3108–3133. https://doi.org/10.1039/C7CS00041C.

(25) Zhang, W.; Hu, Y.; Ge, J.; Jiang, H.-L.; Yu, S.-H. A Facile and General Coating Approach to Moisture/Water-Resistant Metal–Organic Frameworks with Intact Porosity. *J. Am. Chem. Soc.* **2014**, *136* (49), 16978–16981. https://doi.org/10.1021/ja509960n.

(26) Zhang, Y.; Feng, X.; Li, H.; Chen, Y.; Zhao, J.; Wang, S.; Wang, L.; Wang, B. Photoinduced Postsynthetic Polymerization of a Metal-Organic Framework toward a Flexible Stand-Alone Membrane. *Angew. Chem.* **2015**, *127* (14), 4333–4337. https://doi.org/10.1002/ange.201500207.

(27) Tehfe, M.; Louradour, F.; Lalevée, J.; Fouassier, J.-P. Photopolymerization Reactions: On the Way to a Green and Sustainable Chemistry. *Applied Sciences* **2013**, *3* (2), 490–514. https://doi.org/10.3390/app3020490.

(28) Saroyan, H.; Kyzas, G.; Deliyanni, E. Effective Dye Degradation by Graphene Oxide Supported Manganese Oxide. *Processes* **2019**, *7*, 40. https://doi.org/10.3390/pr7010040.

(29) Rauf, M. A.; Meetani, M. A.; Hisaindee, S. An Overview on the Photocatalytic Degradation of Azo Dyes in the Presence of TiO2 Doped with Selective Transition Metals. *Desalination* **2011**, *276* (1), 13–27. https://doi.org/10.1016/j.desal.2011.03.071.

(30) Kalaj, M.; Denny, M. S.; Bentz, K. C.; Palomba, J. M.; Cohen, S. M. Nylon–MOF Composites through Postsynthetic Polymerization. *Angew. Chem. Int. Ed.* **2019**, *58* (8), 2336–2340. https://doi.org/10.1002/anie.201812655.

(31) Ghali, M.; Brahmi, C.; Benltifa, M.; Vaulot, C.; Airoudj, A.; Fioux, P.; Dumur, F.; Simonnet-Jégat, C.; Morlet-Savary, F.; Jellali, S.; Bousselmi, L.; Lalevée, J. Characterization of Polyoxometalate/Polymer Photo-composites: A Toolbox for the Photodegradation of Organic Pollutants. *Journal of Polymer Science* **2020**, pol.20200568. https://doi.org/10.1002/pol.20200568.

(32) Ghali, M.; Brahmi, C.; Benltifa, M.; Dumur, F.; Duval, S.; Simonnet-Jégat, C.; Morlet-Savary, F.; Jellali, S.; Bousselmi, L.; Lalevée, J. New Hybrid Polyoxometalate/Polymer Composites for Photodegradation of Eosin Dye. *Journal of Polymer Science Part A: Polymer Chemistry* **2019**, *57* (14), 1538–1549. https://doi.org/10.1002/pola.29416.

(33) Han, L.; Qi, H.; Zhang, D.; Ye, G.; Zhou, W.; Hou, C.; Xu, W.; Sun, Y. A Facile and Green Synthesis of MIL-100(Fe) with High-Yield and Its Catalytic Performance. *New J. Chem.* **2017**, *41* (22), 13504–13509. https://doi.org/10.1039/C7NJ02975F.

(34) Fu, H.; Song, X.-X.; Wu, L.; Zhao, C.; Wang, P.; Wang, C.-C. Room-Temperature Preparation of MIL-88A as a Heterogeneous Photo-Fenton Catalyst for Degradation of Rhodamine B and Bisphenol a under Visible Light. *Materials Research Bulletin* **2020**, *125*, 110806. https://doi.org/10.1016/j.materresbull.2020.110806.

(35) Lv, H.; Zhao, H.; Cao, T.; Qian, L.; Wang, Y.; Zhao, G. Efficient Degradation of High Concentration Azo-Dye Wastewater by Heterogeneous Fenton Process with Iron-Based Metal-Organic Framework. *Journal of Molecular Catalysis A: Chemical* **2015**, *400*, 81–89. https://doi.org/10.1016/j.molcata.2015.02.007.

(36) Farsani, M.; Yadollahi, B. Synthesis, Characterization and Catalytic Performance of a Fe Polyoxometalate/Silica Composite in the Oxidation of Alcohols with Hydrogen Peroxide. *Journal of Molecular Catalysis A: Chemical* **2014**, *392*. https://doi.org/10.1016/j.molcata.2014.05.001.

(37) Chaturvedi, G.; Kaur, A.; Umar, A.; Khan, M. A.; Algarni, H.; Kansal, S. K. Removal of Fluoroquinolone Drug, Levofloxacin, from Aqueous Phase over Iron Based MOFs, MIL-100(Fe). *Journal of Solid State Chemistry* **2020**, *281*, 121029. https://doi.org/10.1016/j.jssc.2019.121029.

(38) Hindocha, S.; Poulston, S. Study of the Scale-up, Formulation, Ageing and Ammonia Adsorption Capacity of MIL-100(Fe), Cu-BTC and CPO-27(Ni) for Use in Respiratory Protection Filters. *Faraday Discuss.* **2017**, *201*, 113–125. https://doi.org/10.1039/C7FD00090A.

(39) Ren, G.; Zhao, K.; Zhao, L. A Fenton-like Method Using ZnO Doped MIL-88A for Degradation of Methylene Blue Dyes. *RSC Adv.* **2020**, *10* (66), 39973–39980. https://doi.org/10.1039/D0RA08076D.

(40) Bechiri, O.; Abbessi, M. Catalytic Oxidation of Naphtol Blue Black in Water: Effect of Operating Parameters and the Type of Catalyst. *Journal of Water and Environmental Nanotechnology* **2017**, *2* (1), 9–16. https://doi.org/10.7508/jwent.2017.01.002.

(41) Onder, S.; Celebi, M.; Altikatoglu, M.; Hatipoglu, A.; Kuzu, H. Decolorization of Naphthol Blue Black Using the Horseradish Peroxidase. *Appl Biochem Biotechnol* **2011**, *163* (3), 433–443. https://doi.org/10.1007/s12010-010-9051-8.

(42) Zhang, H.; Liu, D.; Ren, S.; Zhang, H. Kinetic Studies of Direct Blue Photodegradation over Flower-like TiO2. *Res Chem Intermed* **2017**, *43* (3), 1529–1542. https://doi.org/10.1007/s11164-016-2713-6.

(43) Cai, T.; Yue, M.; Wang, X.; Deng, Q.; Peng, Z.; Zhou, W. Preparation, Characterization, and Photocatalytic Performance of NdPW12O40/TiO2 Composite Catalyst. *Chinese Journal of Catalysis* **2007**, *28* (1), 10–16. https://doi.org/10.1016/S1872-2067(07)60007-2.

(44) Senasu, T.; Nanan, S. Photocatalytic Performance of CdS Nanomaterials for Photodegradation of Organic Azo Dyes under Artificial Visible Light and Natural Solar Light Irradiation. *J Mater Sci: Mater Electron* **2017**, *28* (23), 17421–17441. https://doi.org/10.1007/s10854-017-7676-x.

(45) Pedrosa, M.; Da Silva, E. S.; Pastrana-Martínez, L. M.; Drazic, G.; Falaras, P.; Faria, J. L.; Figueiredo, J. L.; Silva, A. M. T. Hummers' and Brodie's Graphene Oxides as Photocatalysts for Phenol Degradation. *Journal of Colloid and Interface Science* **2020**, *567*, 243–255. https://doi.org/10.1016/j.jcis.2020.01.093.

(46) Tang, L.; Jia, C.; Xue, Y.; Li, L.; Wang, A.; Xu, G.; Liu, N.; Wu, M. Fabrication of Compressible and Recyclable Macroscopic G-C3N4/GO Aerogel Hybrids for Visible-Light Harvesting: A Promising Strategy for Water Remediation. *Applied Catalysis B: Environmental* **2017**, *219*, 241–248. https://doi.org/10.1016/j.apcatb.2017.07.053.

(47) Cutié, S. S.; Henton, D. E.; Powell, C.; Reim, R. E.; Smith, P. B.; Staples, T. L. The Effects of MEHQ on the Polymerization of Acrylic Acid in the Preparation of Superabsorbent Gels. *Journal of Applied Polymer Science* **1997**, *64* (3), 577–589. https://doi.org/10.1002/(SICI)1097-4628(19970418)64:3<577::AID-APP14>3.0.CO;2-V.

(48) Liang, J.; Liu, F.; Li, M.; Liu, W.; Tong, M. Facile Synthesis of Magnetic Fe3O4@BiOI@AgI for Water Decontamination with Visible Light Irradiation: Different Mechanisms for Different Organic Pollutants Degradation and Bacterial Disinfection. *Water Research* **2018**, *137*, 120–129. https://doi.org/10.1016/j.watres.2018.03.027.

(49) Das, M. C.; Xu, H.; Wang, Z.; Srinivas, G.; Zhou, W.; Yue, Y.-F.; Nesterov, V. N.; Qian, G.; Chen, B. A Zn4O-Containing Doubly Interpenetrated Porous Metal–Organic Framework for Photocatalytic Decomposition of Methyl Orange. *Chem. Commun.* **2011**, *47* (42), 11715. https://doi.org/10.1039/c1cc12802g.